Simulation of Spontaneous Condensation of Viscous Steam Flow in Low-Pressure Convergent-Divergent Nozzles

Dr. Assim H Yousif * ,Dr Kassim K Abbas & Dr Aqeel M Jary ***

Abstract

The present study describes the results of experimental and numerical investigation of wet steam flow in low-pressure convergent-divergent nozzles and deals with the effects of turbulence on the process of homogeneous condensation. The experimental investigation consist mainly the axial pressure distribution of a fixed nozzle test section. The mathematical model that described the droplet nucleation and the growth rates combined with the field conservations was treated numerically within the CFD code FLUENT 6.3., in which the computational domain is discretized in a general unstructured mesh that is locally refined especially in the area of the spontaneous nucleation zone. The equations describing droplet formations and interphase change are solved sequentially after solving the main flow conservation equations. The calculations were carried out assuming that the flow is two-dimensional, compressible, turbulent and viscous. The aim of the present study is the use of the modified k-ε model for modeling the turbulence within an unstructured mesh solver. The results obtained from the numerical part of the current analysis are compared with the experimental results and gave an acceptable agreement. Also present experimental and numerical results showed good agreements with numerical and experimental existing published data.

محاكاة التكثيف التلقائي لجريان البخار اللزج في أبواق تقاربيه تباعديه ذات ضغوط واطئة

الخلاصة

تصف الدراسة الحالية النتائج التجريبية والنظرية لجريان البخار الرطب في بوق تقاربي تباعدي منخفض الضغط وتأثير الاضطراب على عملية التكاثف المتجانس. يتناول الجانب العملي إجراء قياس لتوزيع الضغط المحوري لمقطع اختبار بوق ثابت. آما الجانب النظري فيصف عملية تكون القطرات ومعدل نموها المرافقة لعملية تحول حقل الجريان, وتم معاملة الجانب النظري عدديا باستخدام (CFD code FLUENT 6.3), إذ تم تقطيع المدى الحسابي بواسطة شبكة لاهيكلية شاملة يتم تنعيمها في منطقة نشوء القطرات التلقائي موقعيها. آما المعادلات التي تصف نشوء القطرات وتغير الطور فقد تم حلها بواسطة معادلات التحويل الرئيسية. كما إن الحسابات جرت مع فرض آن الجريان ذي بعدين باستخدام نموذج (k-ε) لمطور لنمذجة الاضطراب مع استخدام الحل المتاح في البرنامج الخاص بالشبكة الاهكلية. إن النتائج المستحصلة حسابيا تم مقارنتها مع النتائج لعملية وأعطت توافقا مقبولا. وبينت المقارنة بين النتائج النظرية والعملية الحالية والنتائج السابقة المنشورة تطابقا جيدا.

* Mechanical Engineering Department ,University of Technology/Baghdad
** Electromechanical Engineering Department ,University of Technology/Baghdad
*** Ministry of Sciences and Technology/Baghdad

Eng. & Tech. Journal, Vol. 27, No.13,2009

Simulation of Spontaneous Condensation of Viscous Steam Flow in Low-Pressure Convergent- Divergent Nozzles

Introduction

Modeling wet steam is of practical importance in a number of engineering fields such as low pressure turbines. One of the differentiating features of steam turbines from other turbomachinery is the presence of liquid water in the flow. This line. The expansion process causes the superheated dry steam to first subcool and then nucleates to form a two – phase mixture of saturated vapor and fine liquid droplets known as wet steam. [Young, 1982].

Two phase flows in convergent - divergent nozzles in the existing study were modeled ignoring the effects of viscosity and turbulence. Therefore the objective of the present paper is to study the effects of flow turbulence on the process of spontaneous condensation of supercooled steam.

Experimental set-up

The nozzle flow apparatus unit has been designed to permit a comprehensive study of the with steam at a pressure of up to 700 kN/m^2 .The inlet connections are arranged laws which govern the flow of a nozzle, as in a steam turbine. The inlet chest may be supplied at right angles to each other and each equipped with a throttling valve to regulate the flow into the chest.

The test section (convergent-divergent nozzle) is screwed into a seating in the center of the inlet chest. The following Fig.1 shows the dimensions of the nozzle. To enable the pressure variation along the nozzle to be observed a stainless steel search tube (probe) of nominal diameter (3.31mm) can be traversed along the nozzle axis. A cross drilling of diameter (1.0 mm) in the wall of the probe transmits the local pressure to a high–grade pressure gauge mounted on the probe carrier. The probe is traversed in

leads to a reduction of turbine efficiency and to mechanical damage of the turbine components.[Senoo and White, 2006]. During the rapid expansion of steam a condensation process will take place shortly after the state path crosses the vapor-saturation

increments of (2mm) by rotating a calibrated dial. A pointer attached to the probe carrier moves over a replica of the nozzle profile in order to indicate the position of the measuring point in the nozzle.

At the upper limit of its travel the pressure sensing hole is well clear of the nozzle and registers the inlet chest pressure while at its lower limit it registers the pressure downstream of the nozzle .The length of the probe is such that it projects well beyond the downstream end of the nozzle irrespective of the position of the setting dial.

The nozzle discharges into a vertical tube of large bore fitted with a throttling valve by which downstream or back pressure may be regulated. The chest also carries mercury –in-glass thermometer in an oil pocket, a pressure gauge for indicating the chest pressure and a simple throttling calorimeter for the dryness fraction of the steam.

The discharge from the downstream of the back pressure throttling valve is directed into a condenser. The condenser through a two-way cock by which it may either be derived to waste or to a suitable measurement vessel and a flow control valve are provided on the side of the condenser.

Steam calculation in experimental part

Steam velocity calculation along the length of the nozzle is done according to the perfect gas low where the pressure and volume are related by the simple

Eng. & Tech. Journal, Vol. 27, No.13,2009

Simulation of Spontaneous Condensation of Viscous Steam Flow in Low-Pressure Convergent- Divergent Nozzles

expression, PV^γ = constant. Steam deviates from the laws of perfect gas. The P-V relationship is given by:

PV^n = constant   ….(1)

Where:

n = 1.135 for saturated steam,

n =1.3 for superheated steam, and

n = **[1.035 + 0.1χ]**   for wet steam.

Where

χ is the initial dryness fraction of the steam.

The velocity through the nozzle is a function of the pressure-differential across the nozzle.

$$V_x = \sqrt{\frac{2n[P_1 n_1 - P_x n_x]}{(n-1)}} \quad ….(2)$$

Where:

x represents the distance between a point on the nozzle axis and the inlet nozzle, (P_1, P_x) is the magnitude of the pressure that measured by the pressure gauge, and (n) is the inlet steam specific volume.

As the pressure downstream of the nozzle falls to a value equals to or is below the critical pressure that corresponds to the total pressure upstream, is determined by the following equation:

$$\frac{P_c}{P_1} = \left(\frac{2}{n+1}\right)^{\left(\frac{n}{n-1}\right)} \quad ….(3)$$

Sound velocity and Mach number through the nozzle were obtained according to the following equations:

$$Vsx = \sqrt{nP_x n_x} \quad …(4)$$

$$M_x = \frac{V_x}{V_{sx}} \quad …..(5)$$

Numerical implementation

The mathematical model of homogeneous condensation in wet steam flow is based on the physical model, which implemented by a general CFD Code FLUENT 6.3. These are namely

thermodynamic non-equilibrium, which can occur in case of quick expansion of the steam flow. This state is characterized by subcooling of steam, when the steam temperature is lower than the equilibrium temperature of saturated steam for the given pressure.

The wet steam is a mixture of two phases, the primary phase is the gaseous - phase consisting of water vapor (denoted by the subscript *g*) while the secondary phase is the liquid-phase consisting of condensed water droplets (denoted by the subscript **l**). [Sejna and Eaineg. 1994].

The following assumptions are made in this model for simplicity of the present analysis, no slip velocity between the droplets and Vapor surrounding them, the interactions between droplets are neglected, the wetness mass fraction is small, less than 20%, and the liquid phase consists of droplets whose radii are on order of 1μm or less. From the preceding assumptions, the following equations can be adopted [Sejna and Eaineg. 1994].

$$r = \frac{r_g}{(1-b)} \quad ….(6)$$

$$\frac{\partial rb}{\partial t} + \tilde{N} \cdot (rVb) = G \quad ….(7)$$

$$\frac{\partial rh}{\partial t} + \tilde{N} \cdot (rVh) = rI \quad ….(8)$$

Also the following assumption suggested to the phase change model, the condensation is homogeneous ,the droplet growth is based on average or mean radius, the droplet surrounding is infinite vapor space, spherical droplet shape assumption and the heat capacity of the droplet is neglected comparison with the releasing of latent heat occur in condensation [Young, 1982].

$$G = \frac{4}{3}pr_l I r^{*3} + 4pr_l h\bar{r}^2 \frac{\partial \bar{r}}{\partial t} \quad ….(9)$$

Eng. & Tech. Journal, Vol. 27, No.13,2009

Simulation of Spontaneous Condensation of Viscous Steam Flow in Low-Pressure Convergent- Divergent Nozzles

Where $\bar{r}$ is the average radius of the droplet, and r^* is the Kelvin-Helmholtz critical droplet radius which given by:

$$r^* = \frac{2S}{r_l RTg\ln S} \qquad \dots(10)$$

Where

$$S = \frac{P}{Rs(Tg)} \qquad \dots(11)$$

The condensation process involves two mechanisms, the mass transport from the vapor to the droplets and heat transfer from the last to the surrounding in the form of latent heat. This energy balance can be written as:

$$\frac{d\bar{r}}{dt} = \frac{RCp(g+1)}{2gr_l h_{lg}\sqrt{2pRTg}}\left(T_l - Tg\right) \qquad \dots(12)$$

The nucleation rate described by the steady-state classical homogeneous nucleation theory and corrected for non-isothermal effects, is given by

$$I = \frac{q_c}{1+q}\left(\frac{2S}{pm^3}\right)^{\frac{1}{2}}\frac{r_g^2}{r_l}\exp\left(-\frac{4pr^{*2}S}{3KTg}\right) \qquad \dots(13)$$

Where

$$q = 2\frac{(g-1)}{(g+1)}\frac{h_{lg}}{RTg}\left(\frac{h_{lg}}{RTg} - \frac{1}{2}\right) \qquad \dots(14)$$

The equation of the vapor phase is given by the following viral equation [Young 1988]:

$$P = r_g RT(1 + A_1 r_g + A_2 r_g^2) \qquad \dots(15)$$

Where A_1 (is given in (m^3/kg)) and A_2 (is given in (m^6/kg^2)) are the second and the third viral coefficients given by the following relations [Young 1988].

$$A_1 = [\frac{0.0015}{(1+0.0001B)} - 0.000942e^B]*$$
$$[1 - e^{-B}] - 0.0004882B \qquad \dots(16)$$

and

$$A_2 = 1.772(C - 0.8978)\exp(-11.16C)$$
$$+1.5\times10^{-6} \qquad \dots(17)$$

Where
B = 1500/T and C = T/647.286 with T, given in K^o.

The mixture properties are computed using the following mixing relation:

$$f = bf_l + (1 - b)f_g \qquad \dots(18)$$

Where f represents any of the following mixture thermodynamic properties: enthalpy, entropy, specific heat, dynamic viscosity or thermal conductivity.

Turbulence model

In the current study the modified (**K-ε**) turbulence model [Yang & Shih (1993)] was adapted when the turbulent model was employed. The enhancement wall treatment potation has been selected to deal with the resolution of the boundary layer in present model. There are three regions treated in the boundary layer, laminar sub-layer $y^+ < 5$, buffer region $5 < y^+ < 30$ and fully turbulent $y^+ > 30$.

Where the symbol y^+, is a mesh-dependent dimensionless distance that quantifies to what degree of wall layer is resolved .After doing the calculations the value of y^+ is observed for each mesh. The values of y^+ are dependent on the resolution of the grid and the Reynolds number of the flow, and are meaningful only in boundary layers. The value of y^+ in the wall-adjacent cells dictates how wall shear stress is calculated. The equation for y^+ is

Eng. & Tech. Journal, Vol. 27, No.13,2009

Simulation of Spontaneous Condensation
of Viscous Steam Flow in Low-Pressure
Convergent- Divergent Nozzles

$$y^+ = \frac{y}{m}\sqrt{r t_w} \qquad ....(19)$$

Where **y**, is the distance from the wall to the cell center, m is the molecular viscosity, r is the density of the mixture, and t_w is the wall shear stress. In the turbulence specification method drop-down list, select turbulent viscosity ratio. For low to moderate inlet turbulence, a viscosity ratio of unity is recommended. Accept the default value of 10 for backflow turbulent viscosity ratio, but if substantial backflow occurs at the outlet, the backflow values must be adjust to levels close to the actual exit conditions.

Losses calculation

In the current study, the kinetic energy loss coefficient definitions is employed as given in [Dykas (2001] as follows:

$$Z_{E_K} = \frac{C_2^2/2}{h_{10} - h_{2s}}$$

In addition to this loss coefficient, the thermal efficiency h_T is introduced as follow:

$$h_T = \frac{h_{10} - h_2}{h_{10} - h_{2s}}$$

For these calculations, Specific enthalpy and entropy of steam were calculated on the basis of the parameters obtained as the mass averaged at the inlet and at the outlet.

Choosing solver

In the present study, the coupled implicit solver is selected because it is the only solver available for wet steam model. After choosing the solver type the operation procedure was done generally as follows:

ⓐ Import and scale mesh file.

ⓑ Select physical models.

ⓒ Define material properties.

ⓓ Prescribe operating conditions.

ⓔ Prescribe boundary conditions.

ⓕ Provide an initial solution.

ⓖ Set solver controls.

ⓗ Set up convergence monitors.

ⓘ Compute and monitor solution.

ⓙ Analysis

The Reynolds-averaged Navier - Stokes equations are solved for two-phase flow mixture (wet steam), using a finite volume method on an unstructured and adaptive mesh. These equations are linked with spontaneous nucleation equations and with equations describing growth of homogeneous water droplets and the modified (**K-ε**) turbulence model was used to model the turbulence.

Results and discussions

The geometry and numerical grid of the nozzle apparatus which used in the experimental side are shown in figures (2) and (3) .The experimental pressure distribution was measured along center line of the nozzle side wall and the theoretical treatment used for comparison with the   described in the following section.

Comparisons between the predicted and measured centerline pressure distributions and Mach number are shown in figures from (6) to (9) for nozzle apparatus. The agreement between the calculated pressure traverses and the measured value is good.

Figures (6 to 9) show predicted and measured variations in pressure along nozzle, when the total pressure in the nozzle inlet was fixed, whereas the back pressure values were changed. Therefore, these figures mentioned above demonstrate the impact of outlet back

Eng. & Tech. Journal, Vol. 27, No.13,2009

**Simulation of Spontaneous Condensation
of Viscous Steam Flow in Low-Pressure
Convergent- Divergent Nozzles**

pressure on the process of spontaneous condensation.

Figures (4) and (5) show pressure distribution and isolines for back pressure values of (0.7) bar and (0.5) bar. The calculated courses of the pressure relative to inlet total pressure along the length of the nozzle are visible from these figures Figure (6) shows the comparison of pressure ratio distribution of theoretical and experimental results, while in figure (7) there is a comparison between theoretical and experimental of Mach number results. Figures (8) and (9) show comparison of both pressure distribution and Mach number distribution between theoretical and experimental results for back pressure values of (0.5) bar and (0.3) bar, the slop of the Mach number distribution curve represents the discrepant behavior of Mach number along the nozzle length relative to that of pressure distribution due to the velocity increasing on account of retreating of pressure.

Existing nozzles

The present numerical solution has been tested with well-known nozzles .Also the numerical results are compared with existing experimental and numerical data obtained by several researchers for the same nozzles. The general procedure employed in the current study for the steam condensing calculations theoretically is the same for all nozzles under study and may be summarized as; total pressure, total temperature and flow direction normal to the boundary were enforced at the nozzle inlet assuming that the flow is symmetrical about the nozzle centerline and symmetry conditions were enforced for all flow variable along this plane. The mass fraction of the liquid phase and the number of liquid droplet per unit volume were set to zero at the nozzle inlet to model dry steam conditions, as was the case in the original experiments. The

calculations were carried out assuming both situations (viscous and inviscid) for steady-state compressible flow. All calculations here were performed on a series of different nozzle geometries and the results show all of the important characteristics of homogeneous nucleation in expanding nozzles.

Ⓐ **Moses and Stein nozzle:** The nozzle geometry was two-dimensional. This nozzle is an arc nozzle with critical throat of 1cm in height, the geometrical shape of this nozzle shown in figure (10). The numerical grid is presented in and the total pressure and total temperature at the inlet of the nozzle for this test case is Po = 70727.52 Pascal and To = 377.150 K respectively. Both Pressure ratio and Mach number are plotted along the nozzle axis in the same figure for both cases viscous and inviscid flows as shown in figures (12) and (13).It can be seen that for pressure ratio or Mach number, the curve that obtained from dry solution was identical with that obtained from wet solution until the nucleation occurs at distance equal to 8.6 cm downstream of the nozzle throat for viscous flow and equal to 8.8 cm downstream of the nozzle throat for inviscid flow.

The homogeneous nucleation with formation of water liquid droplets takes place when both the state exceeds the saturation line and the saturation ratio is larger than unity. This behavior could be observed closely by looking at the distribution of the nucleation rate that described by figure (14) and the distribution of subcooled vapor temperature in the same figure. The start of the nucleation process with created large number of liquid droplets is when the subcooled vapor temperature reaches (16 C°) about (1-cm) upstream of the nozzle throat .The changing in the sign of the subcooled vapor temperature to positive

Eng. & Tech. Journal, Vol. 27, No.13,2009

**Simulation of Spontaneous Condensation
of Viscous Steam Flow in Low-Pressure
Convergent- Divergent Nozzles**

values is at nearly (3-cm) upstream from the nozzle throat in which the flow enters the supersaturation zone. In the diverging region of the nozzle condensation processing increase combined with growth of liquid droplets that formed earlier. In turn, a jump in the static pressure measured as a sign for occurrence deviation in the thermodynamic state due to releasing the heat of evaporation. Figure (15) shows a comparison picture for two wet steam properties, the liquid mass fraction (wetness) and the liquid mass generation rate for two situations (viscous and inviscid flow) .Although the peak of the liquid mass generation rate for inviscid wet steam is larger than of the viscous wet steam but the maximum value of wetness is the same for both cases. Again this is due to the relatively high superheat inlet conditions. The wetness mass fraction increases after the throat. The kinetic loss for inviscid wet steam case is 0.9627 and the thermal efficiency is 56.45% in which it is less than that of inviscid dry case.

Ⓑ **Barschdorff nozzle**: is an arc nozzle with critical throat height 60mm and radius of the wall curvature 584mm. The geometry of this nozzle is plotted in figure (16) and the mesh size is 20 x 120 as shown in figure (17). By comparison of the results of figure (18) obtained from the present study with those of figure (19) obtained by [Dykas 2001] seen that both predicted pressure profiles agree well with experimental measurements. The calculated mean droplet radius slightly differs due to the variation of the method used for both studies where an interpolation of the droplet spectra, can influence the value of calculated mean droplet radius. Heat released by the nucleation slows down the supersonic flow resulting in a pressure jump called the condensation shock. The pressure distributions in these figures show a well

captured position of this pressure jump. Pressure isolines (contour graph) figure (20) shows a very good agreement with numerical results of [Dobes et.al 2004] figure (21). Figure (22) shows the wetness mass fraction contours for inviscid wet steam obtained from present study which compared with that obtained by [Dobes et.al 2004] figure (23). The agreement between them is evident where from both numerical results, the beginning of the liquid mass fraction were at a distance near to $x = 0.043$ m of 0.005 and reach the maximum value 0f 0.045 at the nozzle outlet. Figure (24) shows in the same graph the distributions of both nucleation rate and the mean droplet radius for inviscid and viscous wet steam flows, although the maximum nucleation rate is close for both cases, but the difference is large for the peaks of the average radius. Figure (25) shows another two parameters that specify the wet steam features these are the subcooled vapor temperature and the liquid mass fraction. From this figure, the comparison between the result obtained for both cases (inviscid and viscous flows) shows that, the two subcooling temperature curves are coinciding until approximately $x = - 0.05$ upstream of the throat and the maximum value for both cases take place at $x = 0.05$ downstream of the throat at which, in the other side of this figure and for viscous wet seam flow, the wetness has the onset value near to 0.001 and reach upper value of 0.0425 at the nozzle exit. The kinetic loss for inviscid wet steam case is 1.12055 and the thermal efficiency is 88.02% in which it is less than that of inviscid dry case.

Ⓒ **Meyer nozzle**: Another valuable comparison is with the nozzle geometry and flow conditions of Meyer that was used by [Sejna and Stastny 2007].the geometry and computational grid of this nozzle are given in figures (26)

Eng. & Tech. Journal, Vol. 27, No.13,2009

Simulation of Spontaneous Condensation of Viscous Steam Flow in Low-Pressure Convergent- Divergent Nozzles

and (27) respectively. Figure (28) shows Mach number contours for inviscid wet steam. The flow is supersonic in the diverging portion of nozzle as seen by the Mach number isolines in this figure the so called condensation shock which adds an additional aerodynamic loss similar to that of a mild shock. A direct comparison cannot be made because the Mach number profile across the nozzle is not uniform. Figure (29) presents a contour picture for the variation of the liquid mass fraction along the nozzle length where a sharp rise in wetness fraction after location of nearly $x = 0.38$ m downstream of nozzle throat. Figure (30) displays in one graph a comparison of nucleation rate and wetness distributions for viscous and inviscid wet steam solutions in addition to those obtained by [Sejna and Stastny 2007]. At the nozzle location $x = 0.38$ a sharp rise in wetness fraction is observed, reflecting the rapid growth of the droplets immediately following the peak nucleation. Figure (31) shows a comparison of surface tension of droplet and number of droplets for viscous and inviscid wet steam with those obtained from [Sejna and Stastny 2007] .It can be seen that the effect of viscous on both distributions and the results of adopting both the current inviscid and previous work are identical.. Figure (32) shows the plot of pressure and Mach number distributions for inviscid wet steam obtained by current study with those got by [Sejna and Stastny 2007].The curves have the same shape until nucleation takes place at $x = 0.380$ m downstream of the throat .It is noticed that the agreement between them is good. Figure (33) shows the validation of this CFD code by comparison of the calculated subcooling distribution with that obtained from previous work [Sejna and Stastny 2007] for the same inlet boundary conditions. Both calculated results show that the

subcooling temperature is 15 K at the inlet nozzle and nearly equal to 6 K at nozzle exit. The kinetic loss for

Since the thermodynamic properties database employed can also be used for high pressure applications so a high – pressure nozzle test was also calculated. The boundary conditions reported with inlet total pressure of 10 bars and the inlet stagnation temperature of 486 K was employed. Figures (34) and (35) display the constant contours of pressure ratio and Mach number respectively, while the isolines of wetness fraction are presented in figure (36) .The predicted centerline pressure for both dry and wet steam flow compared together with the Mach number distributions along the nozzle length as shown in figure (37). These figures show a similar behavior to that of the low-pressure calculations was obtained earlier. The nucleation rate is much higher in the high pressure due to the higher density ratio of the vapor to the liquid. As a result, the wetness fraction in the high pressure is larger than that in the low-pressure also due to the higher density of the vapor in the high pressure flow the increased fluid inertia decreases the response to the condensation front as compared to the low pressure case. Inviscid wet steam case is 1.06645 and the thermal efficiency is 86.02% in which it is less than that of inviscid dry case.

Ⓓ **Moore nozzle**: The geometry of nozzle consists of three sections shown in figure (38) while the computational mesh of this nozzle is shown in figure (39). These three sections of nozzle geometry caused a discontinuity in nozzle curvature produces strong two-dimensional effects. Figure (40) shows the predicted centerline pressure ratio, the upper graph is pressure ratio profile while the lower is the isolines of that distribution. The rapid condensation zone takes place at 0.12m further from the

Eng. & Tech. Journal, Vol. 27, No.13,2009

Simulation of Spontaneous Condensation of Viscous Steam Flow in Low-Pressure Convergent- Divergent Nozzles

nozzle throat and the comparison with both the experiment results of [Moore et.al 1973] and the predicted results by [Gerber and Kermani 2004]. Figure (5-41) shows both the profile and contours of Mach number distribution along the nozzle centerline. It is apparent from this graph the flow declines through the nucleation zone. Figure (42) shows the pressure ratio distribution of inviscid wet steam for different back pressures. Figure (43) shows the Mach number distribution .As shown in this figure the flow smoothly accelerates within the converging portion of the nozzle, passes the sonic condition at the throat and continuous accelerating up to M = 1.3 , at which nucleation occurs at location x = 0.042 m. Following the nucleation process, rapid release of latent heat suddenly reduces the frozen Mach number while increasing pressure and the vapor temperature. This rapid response behaves similar to a normal shock wave and is often termed a condensation shock since it takes place in response to homogeneous nucleation in a two-phase system. However, unlike a normal shock, in which the post shock condition is subsonic, in a condensation shock the post shock condition could be sonic at most. Figure (44) shows that the results of static pressure distribution obtained by previous Moore agree with present computations. In the region between the shock and the nucleation onset location, both the liquid mass fraction and droplet size slightly increases as shown in figure (45) and figure (46). After that the decelerating of the subsonic flow experiences a pressure rise, in which the wetness fraction reduces and liquid droplets evaporate to small sizes until vanishes at last. Again from these figures it will be seen that the effect of back pressure on the wet steam flow behavior and its main characteristics such as wetness and droplet radius. Figure (47)

shows the comparison of Mach number for inviscid wet steam at two different outflow boundary condition situations. The same behavior can be seen in figure (48), which shows the same results obtained by [Kermani and Gerber 2003] and a good validity of the present code to capture the condensation shock. Figure (49) shows supercooling distribution of inviscid wet steam along the centerline of nozzle for different back pressures. It is seen that the fluctuations in the supercooled field ΔT following the shock increases and also shows that after peak nucleation , the supercooling level rapidly drops to near equilibrium conditions .This near equilibrium condition prevails the remaining length of the nozzle for the supersonic outflow case. It should be noted that the small positive value of ΔT is a physical requirement to support latent heat release toward the gas phase as condensation continues on the droplet surfaces. As opposed to the supersonic outflow case, the small negative value of ΔT downstream of the shock is a physical requirement to support heat movement toward the liquid phase as evaporation continuous on droplet surfaces. The kinetic loss for inviscid wet steam case is 1.08252 and the thermal efficiency is 40.94% in which it is less than that of inviscid dry case.

Conclusions

By using CFD code Fluent 6.3., the phase change of the homogeneous nucleation and growth of existing droplets were successfully modeled.

The numerical results of pressure distribution in convergent–divergent nozzles captured qualitatively the pressure increase due to sudden heat release by the non-equilibrium condensation and agreed well with experimental data. Also the numerical results of the pressure distributions, droplet growth, nucleation

Eng. & Tech. Journal, Vol. 27, No.13,2009

Simulation of Spontaneous Condensation of Viscous Steam Flow in Low-Pressure Convergent- Divergent Nozzles

rates and wetness are agreed well with existing theoretical and experimental data.

In all results obtained the rapid condensation region has occurred downstream of the throat. This process was accompanied by pressure rise when the flow was supersonic otherwise, it is still occurs downstream of the throat but don't has affection on the pressure. The course of pressure ratio shows a jump at the end of nucleation region due to sudden heat release by the nonequilibrium condensation.

In condensing steam flow both thermodynamic and aerodynamic losses were observed. These losses together case interact each other.

New time scale based model (k-ε) for near-wall turbulence gave a good representation of viscous effect of two phase flow and showed that the droplet nucleation and growth rates results were very close to reality.

List of symbols

A	Cross section area.
g	The bulk Vapor.
h_{lg}	Latent heat.
I	Nucleation rate per unit volume
J	Nucleation rate per unit mass.
k	The thermal conductivity.
K_n	Knudsen number.
l	The bulk liquid.
m	Mass of a condensable vapor molecule.
P	Pressure.
R	Vapor phase specific constant.
r	Droplet radius.
S	Saturation ratio.
T	Temperature.
V	Volume.
b	Wetness factor.
d	Surface tension.
G	Mass generation rate due to condensation
m	Dynamic viscosity.
h	Kinetic viscosity.
ρ	Density.
t	Stress tensor.
g	Ratio of specific heat capacities.
q	Non-isothermal correction factor.

References

[1]Dobes, J., Fort, J. and Halma, J. Numerical Solution of Single –and Two-Phase Transonic Flow in Axial Cascade, *European congress on computational Methods in Applied Sciences and Engineering, ECCOMAS* (24-28 July 2004), pp. 1-19.

[2]Dykas, S., Numerical Calculation of The Steam Condensing Flow. TASK QUARTERLY, Vol. 5, No. 4, PP. 519-535, 2001.

[3]Gerber, A. G. and Kermani, M. J., A pressure based Eulerian-Eulerian multiphase model for non equilibrium condensation in transonic steam flow. *International Journal of Heat and Mass Transfer*, Vol.47, PP.2217-2231. 2004.

[4]Sejna, M. and Eaineg., Numerical Modeling of Wet steam Flow with Homogeneous Condensation on Unstructured Triangular Meshes. *Math. Mech.*, 74 Vol.um 5, PP-375-378. 1994.

[5]Sejna, M. and Stastny, M., The COCHEM FLOW Software Package for Simulating Two-Dimensional Two-Phase Transonic Compressible Flow of Wet Steam with homogeneous & Heterogeneous Condensation, *Version 1.0, PC Progress, Prague*, Czech Republic, 2007.

[6]Senoo, S. and White, A.J., Numerical simulations of unsteady wet steam flows with non- equilibrium condensation in the nozzle and the steam turbine .*ASME Joint U.S.European Fluid Engineering Summer Meeting,* July 17-20, 2006.

[7]Simpson, D. A. and White, A. J., Viscous and unsteady flow calculations of condensing steam in nozzles, *International, J., Heat and Fluid Flow,* Vol.26, PP.71-79., 2005.

[8]Yang, Z. and Shih, T.H., New time scale based $k - e$ model for near – wall turbulence, *AIAA*, J.31 (7), 1191-1197, 1993.

[9]Young, J.B., The spontaneous Condensation on Steam in Supersonic Nozzles, *Physico Chemical Hydrodynamics* .Vol.3, No.2, PP.57-82. 1982.
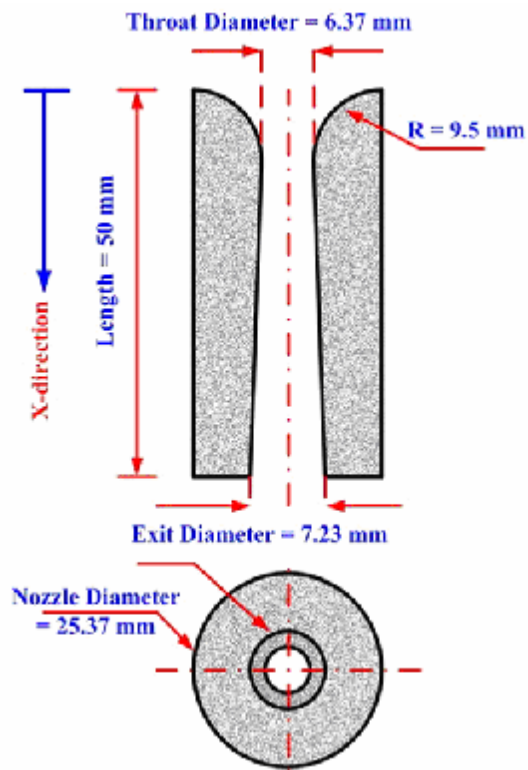
Figure (1) Dimensions of converge divergent nozzle
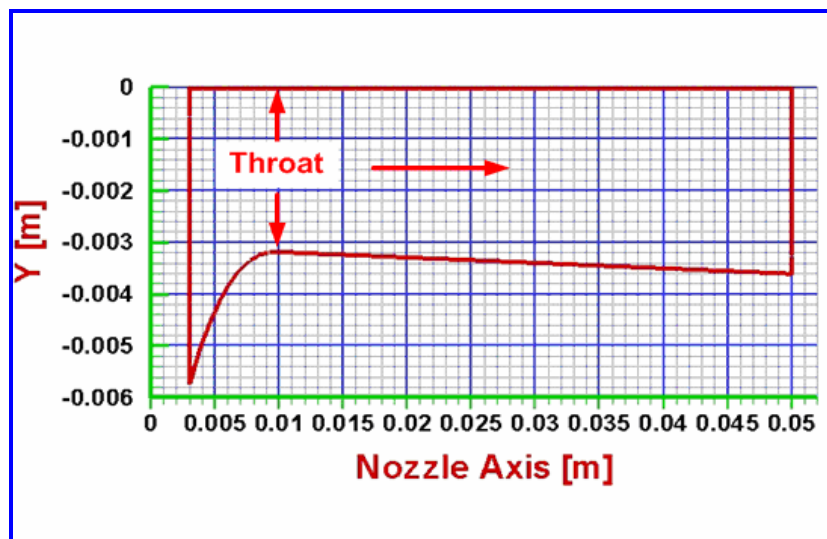
Figure (2) Geometry of nozzle used in experimental work

Eng. & Tech. Journal, Vol. 27, No.13,2009

**Simulation of Spontaneous Condensation
of Viscous Steam Flow in Low-Pressure
Convergent- Divergent Nozzles**
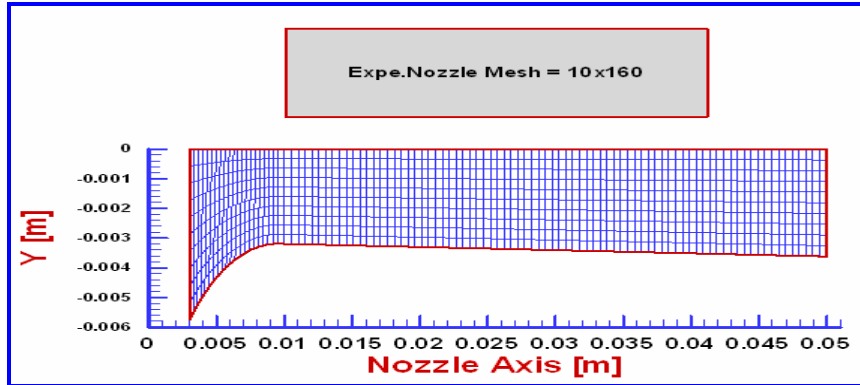
Figure (3) Grid of nozzle used in experimental work
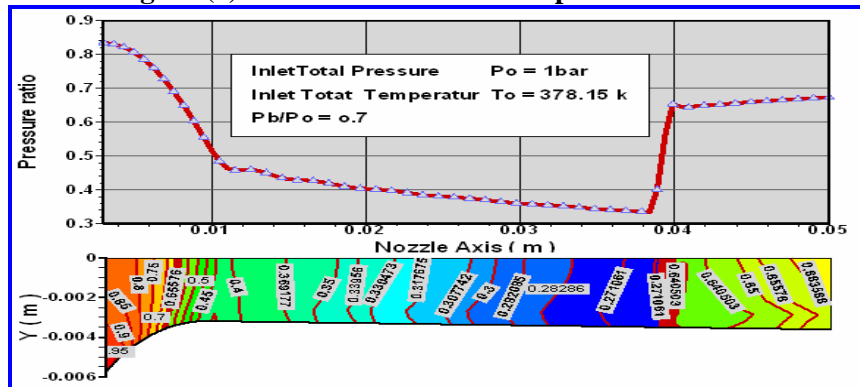
Figure (4) Pressure ratio contours and distribution, theoretical results
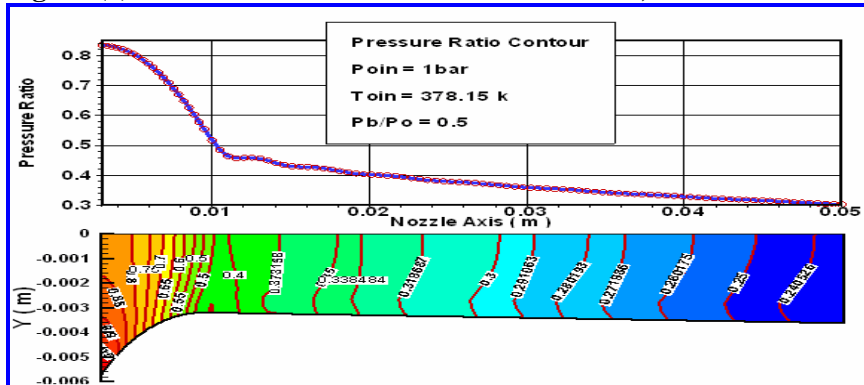
Figure (5) Pressure ratio contours and distribution, theoretical results

Eng. & Tech. Journal, Vol. 27, No.13,2009

Simulation of Spontaneous Condensation
of Viscous Steam Flow in Low-Pressure
Convergent- Divergent Nozzles
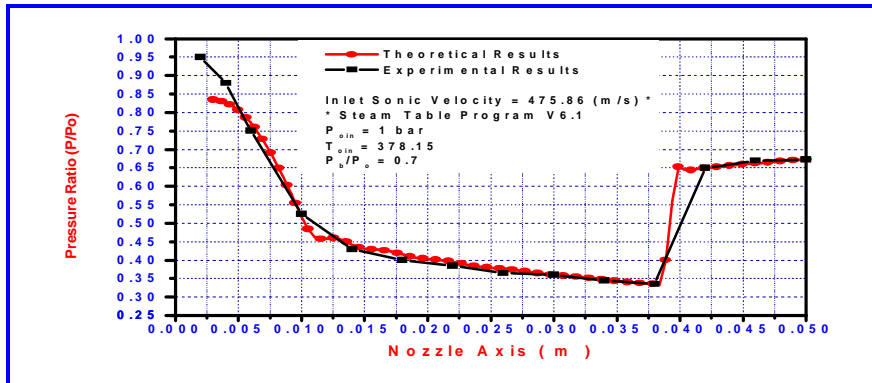
Figure (6) Comparison pressure ratio distribution, theoretical and experimental results
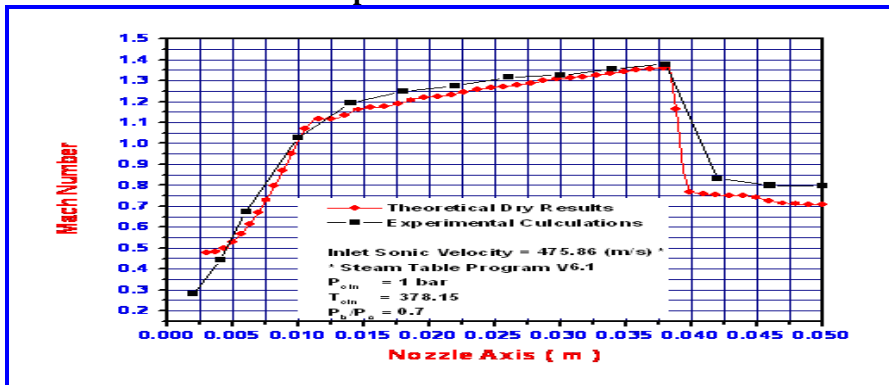
Figure (7) Comparison Mach number distribution, theoretical and experimental results
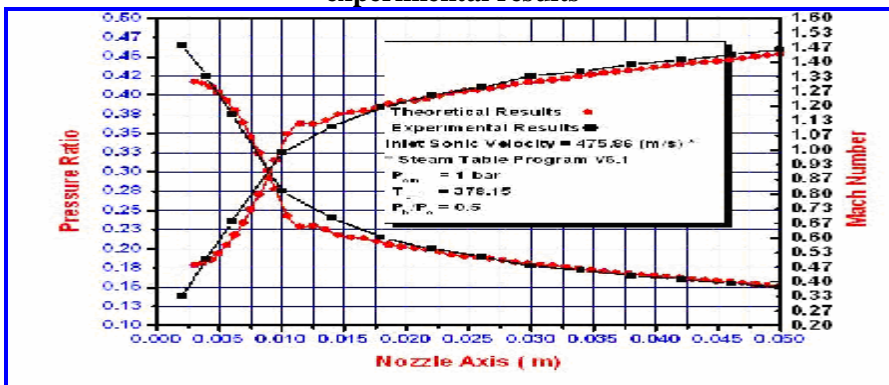
Figure (8) Comparison pressure ratio and Mach number distributions, theoretical and experimental results

Eng. & Tech. Journal, Vol. 27, No.13,2009

Simulation of Spontaneous Condensation
of Viscous Steam Flow in Low-Pressure
Convergent- Divergent Nozzles
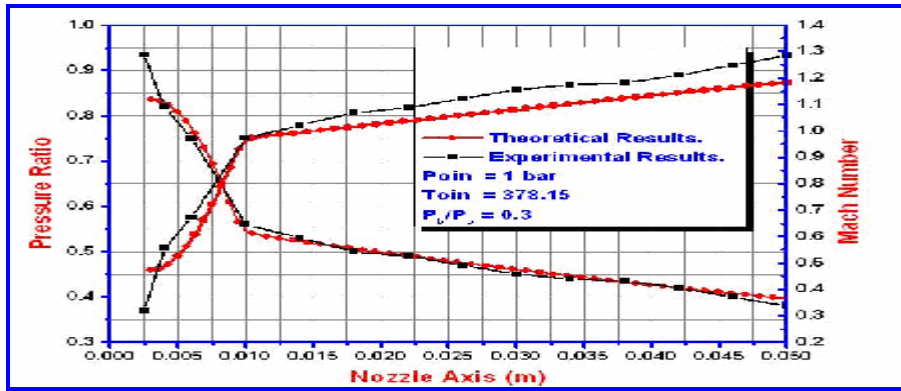
**Figure (9) Comparison pressure ratio and Mach number distributions,
theoretical and experimental results**
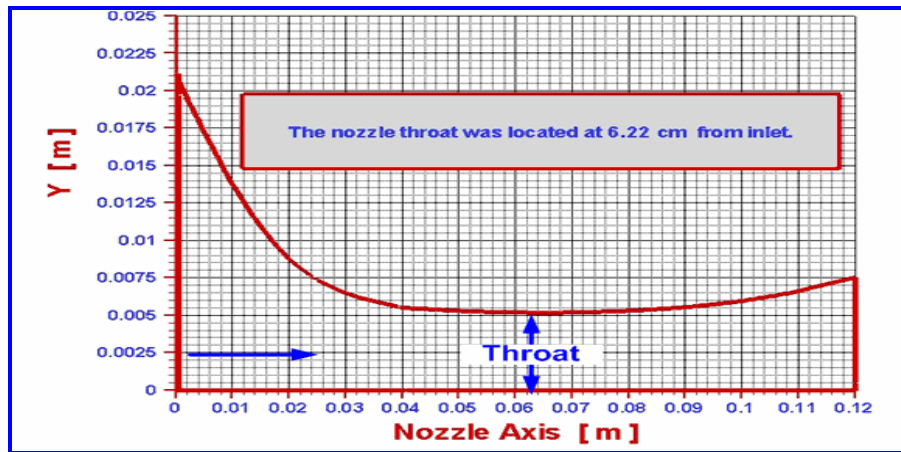
Figure (10) Geometry of Moses nozzle
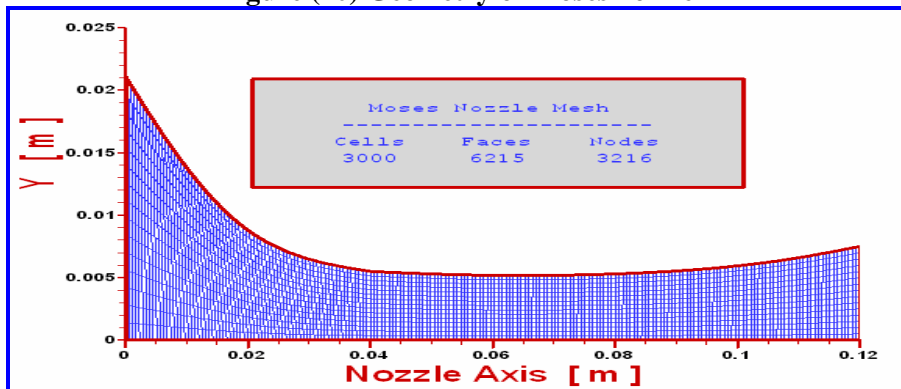
Figure (11) Grid of Moses nozzle

Eng. & Tech. Journal, Vol. 27, No.13,2009

Simulation of Spontaneous Condensation
of Viscous Steam Flow in Low-Pressure
Convergent- Divergent Nozzles
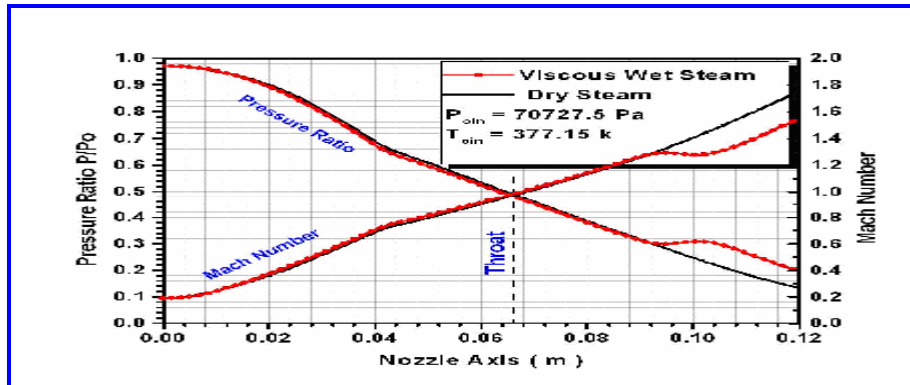
**Figure (12) Pressure ratio & Mach number distribution, viscous, dry steam &
wet Steam**
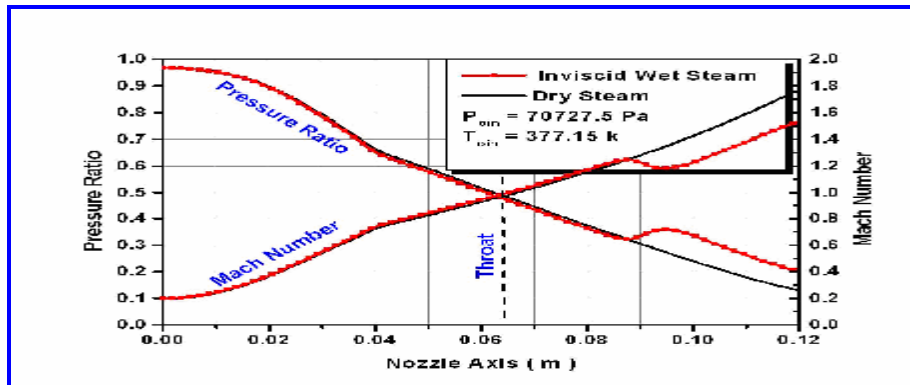
**Figure (13) Pressure ratio and Mach umber distribution, inviscid, dry steam
and wet Steam**
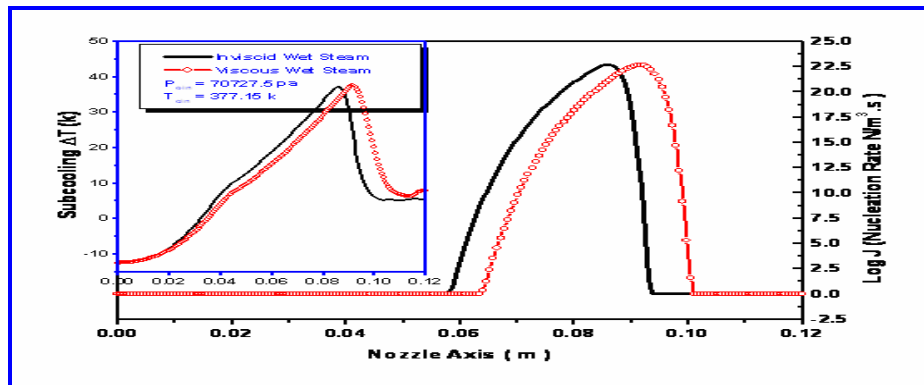
**Figure (14) Comparison of nucleation rate and subcooling, viscous and
inviscid wet steam**

Eng. & Tech. Journal, Vol. 27, No.13,2009

Simulation of Spontaneous Condensation
of Viscous Steam Flow in Low-Pressure
Convergent- Divergent Nozzles
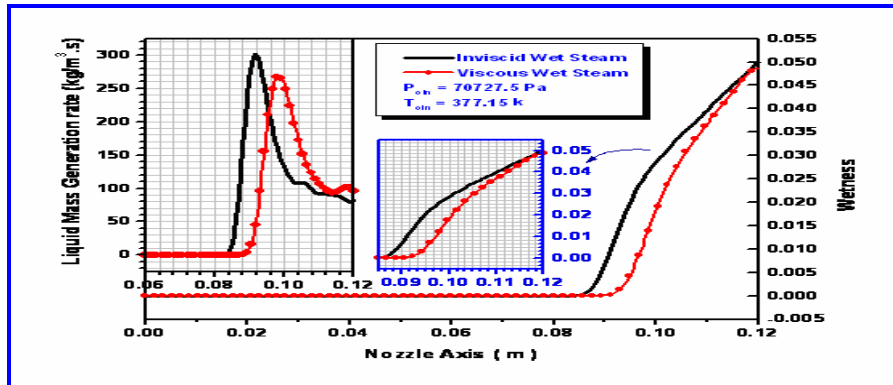
**Figure (15) Comparison of liquid mass generation rate and wetness for
viscous and inviscid wet steam**
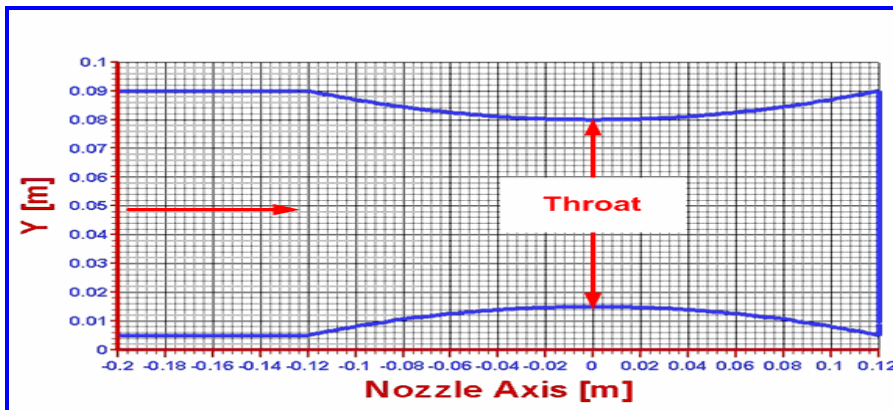
Figure (16) Geometry of Barchdonf nozzle
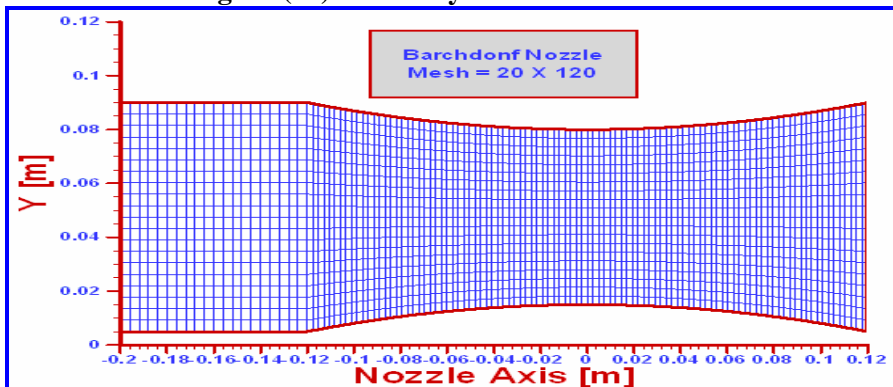
Figure (17) Grid of Barchdonf nozzle

Eng. & Tech. Journal, Vol. 27, No.13,2009

Simulation of Spontaneous Condensation of Viscous Steam Flow in Low-Pressure Convergent- Divergent Nozzles
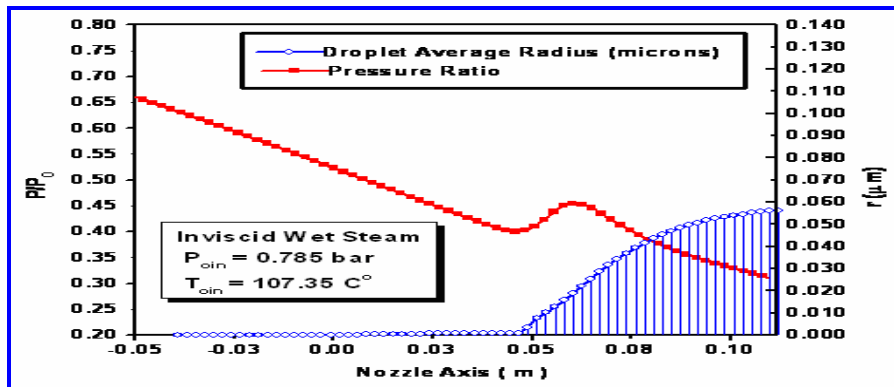
Figure (18) Pressure ratio and droplet radius distribution for inviscid wet steam
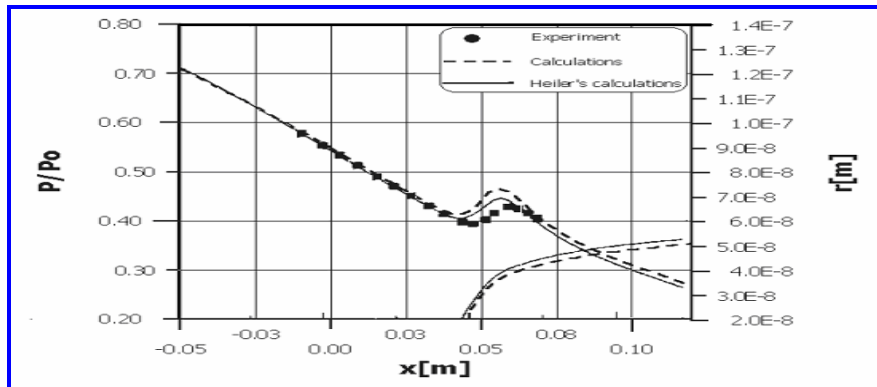
Figure (19) Pressure ratio and droplet radius distribution (P_o = 0.0785 MPa, T_o = 380.55 °K)
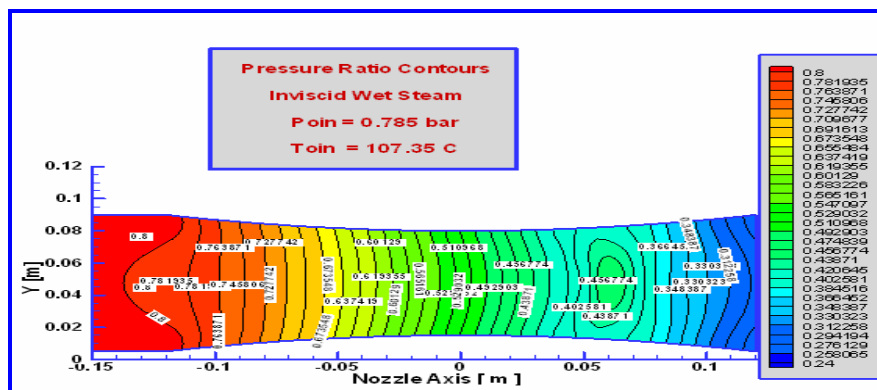
Figure (20) Pressure ratio of isolines for inviscid wet steam

Eng. & Tech. Journal, Vol. 27, No.13,2009

**Simulation of Spontaneous Condensation
of Viscous Steam Flow in Low-Pressure
Convergent- Divergent Nozzles**
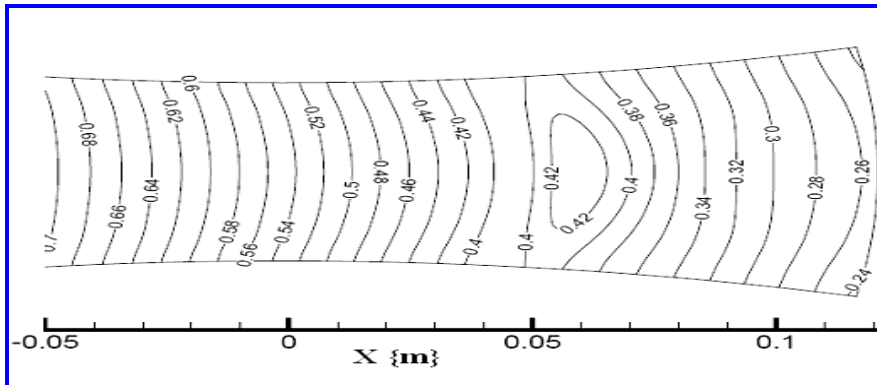
Figure (21) Isolines of P/P_o (ΔP/P_o = 0.02), T_o=380.50 ^{0}K
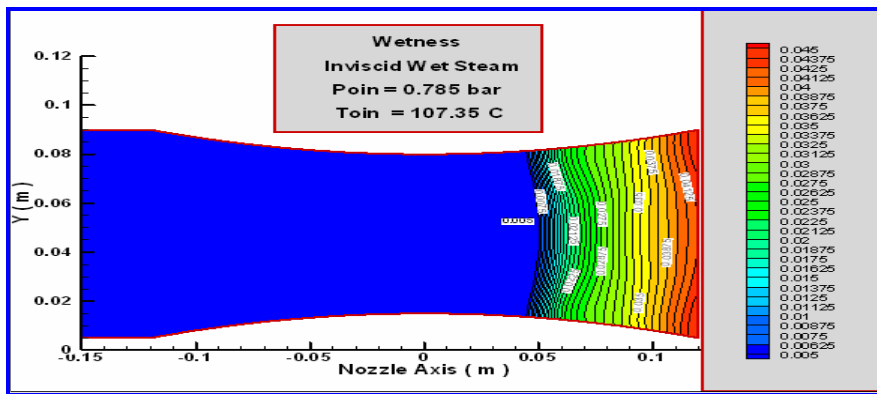
Figure (22) Wetness isolines for inviscid wet steam

Figure (23) Wetness isolines, $\Delta\omega$ =0.005 and P_o=380.50 ^{0}K.

Eng. & Tech. Journal, Vol. 27, No.13,2009

Simulation of Spontaneous Condensation
of Viscous Steam Flow in Low-Pressure
Convergent- Divergent Nozzles
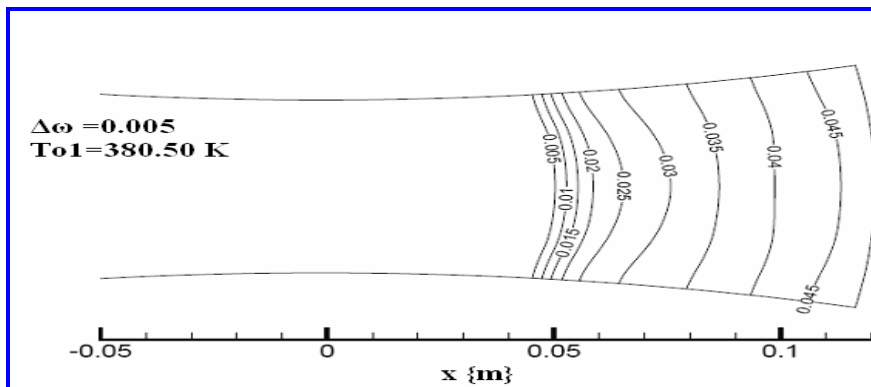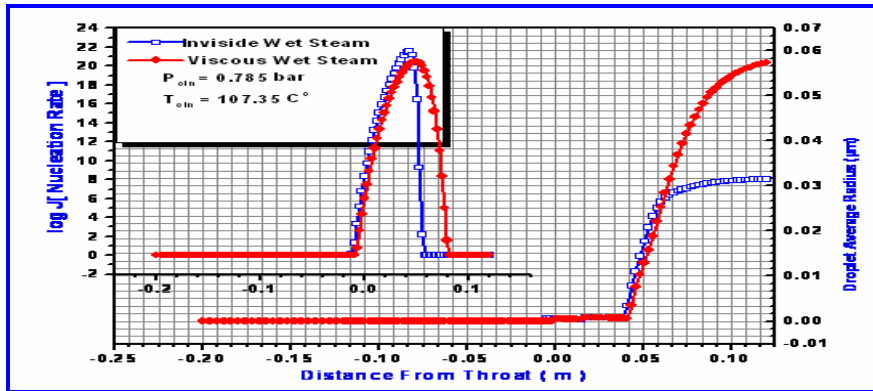
Figure (24) Comparison of nucleation rate and droplet average radius for viscous and inviscid wet steam
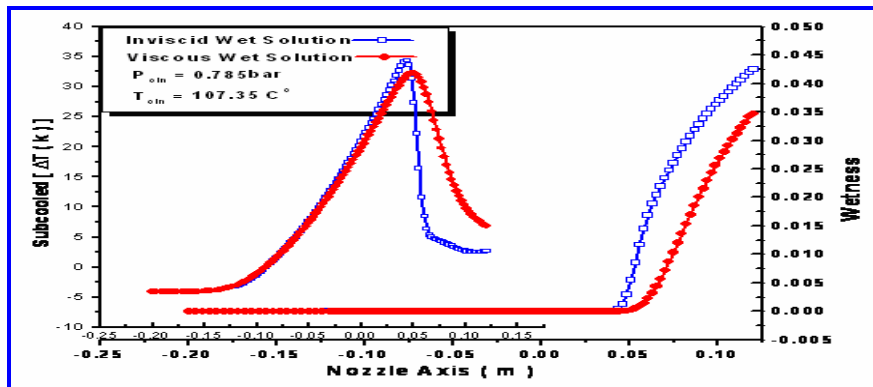
Figure (25) Comparison of subcooled and wetness for viscous and inviscid wet steam
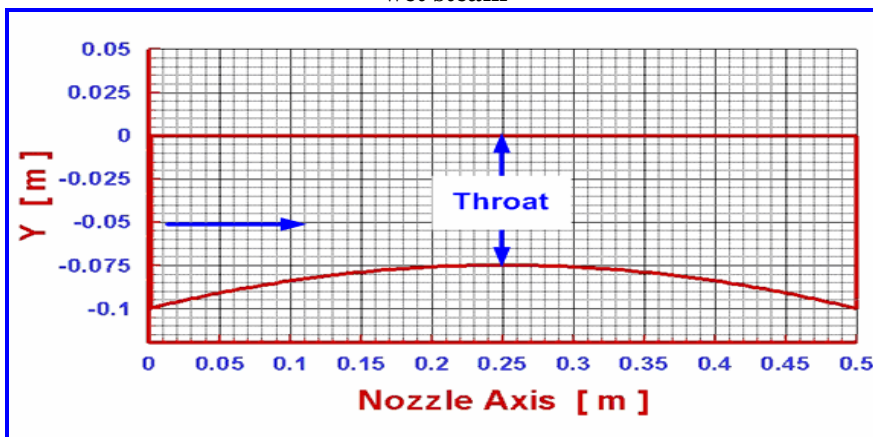
Figure (26) Geometry of Meyer nozzle
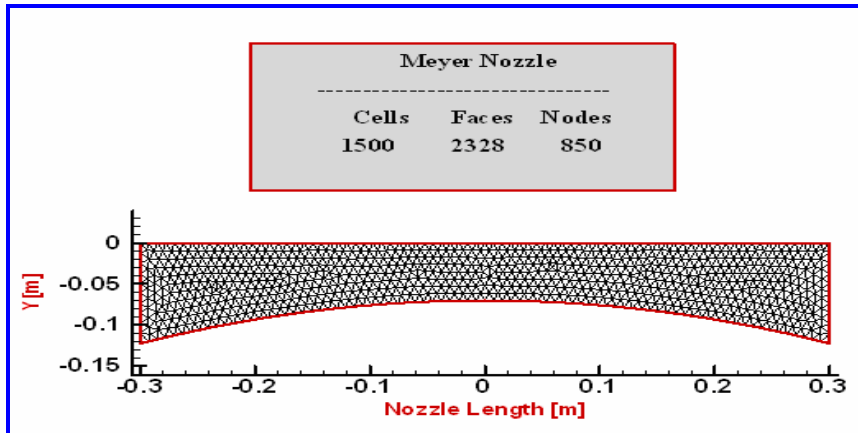
Figure (27) Grid of Meyer nozzle
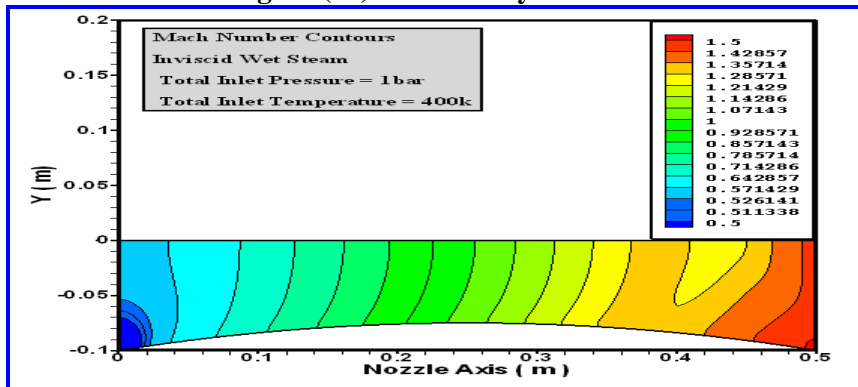
Figure (28) Mach number isolines for inviscid wet steam
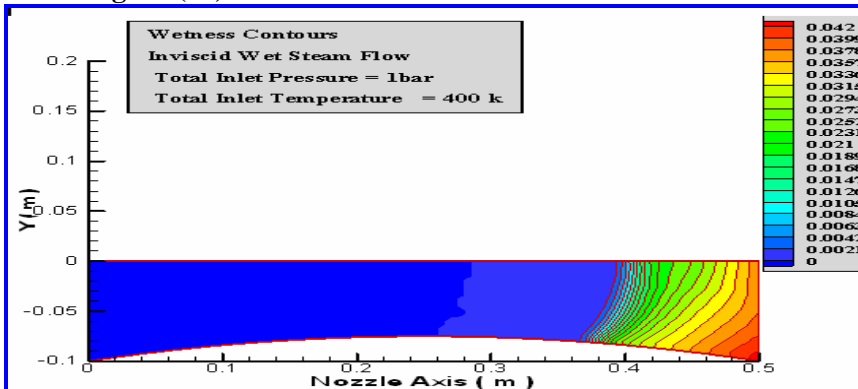
Figure (29) Wetness isolines for inviscid wet steam

Eng. & Tech. Journal, Vol. 27, No.13,2009

Simulation of Spontaneous Condensation of Viscous Steam Flow in Low-Pressure Convergent- Divergent Nozzles
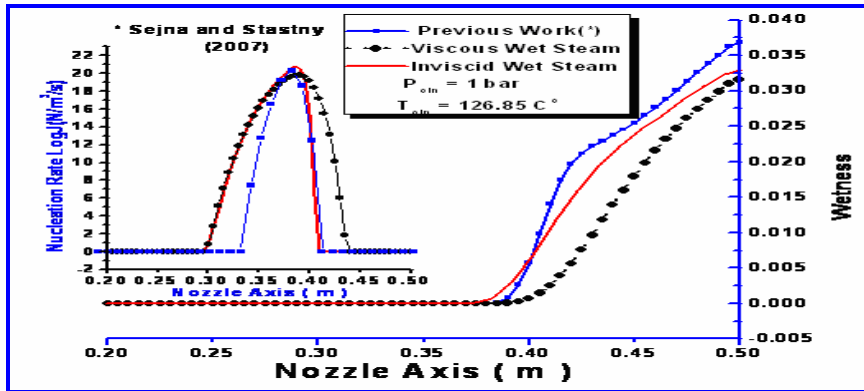
Figure (30) Comparison of nucleation rate and wetness for viscous and inviscid wet steam with other work
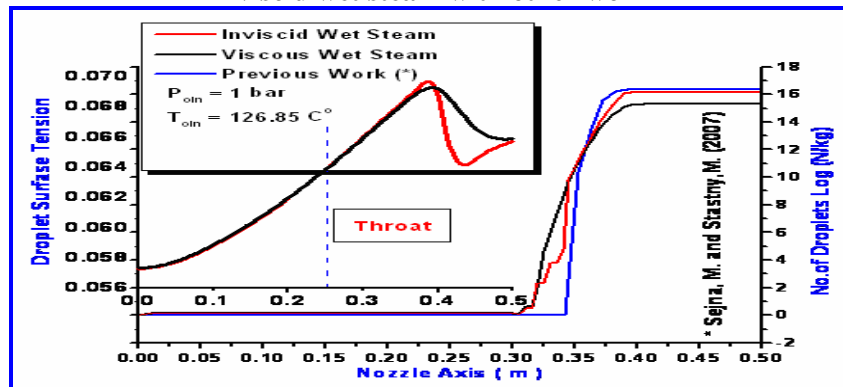
Figure (31) Comparison of surface tension of droplet and number of droplets for viscous and inviscid wet steam
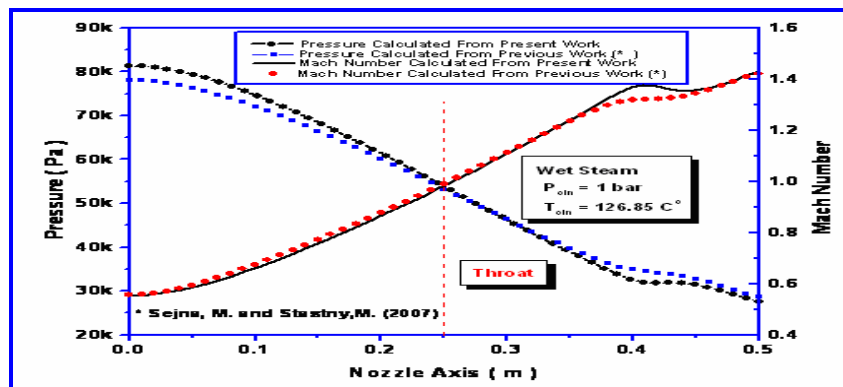
Figure (32) Comparison of pressure distribution and Mach number distribution for inviscid wet steam with other work
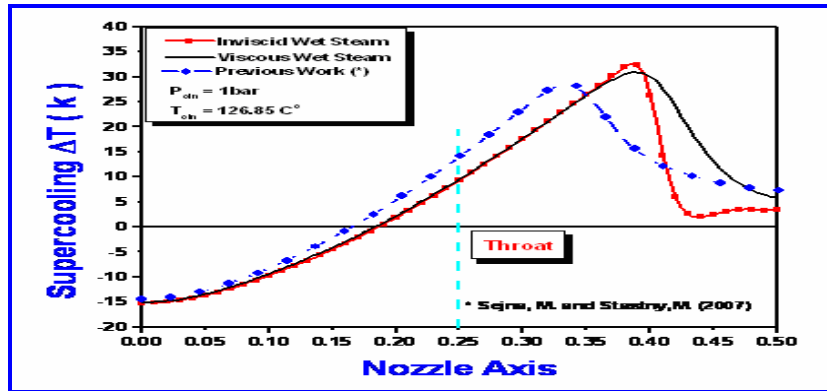
Figure (33) Comparison of subcooling for viscous and inviscid wet steam with other work
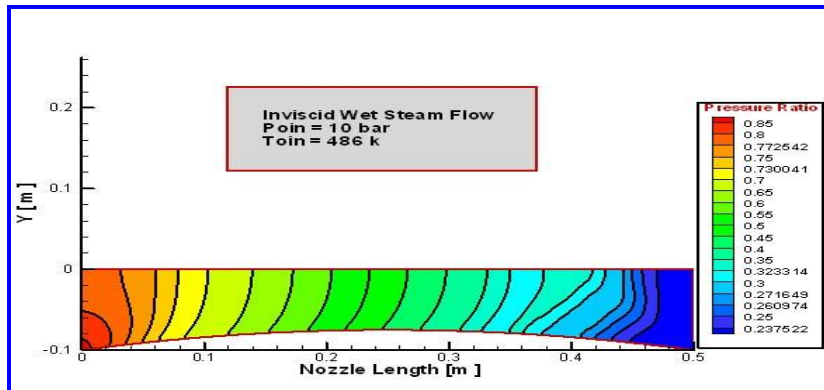
Figure (34) Pressure ratio contours
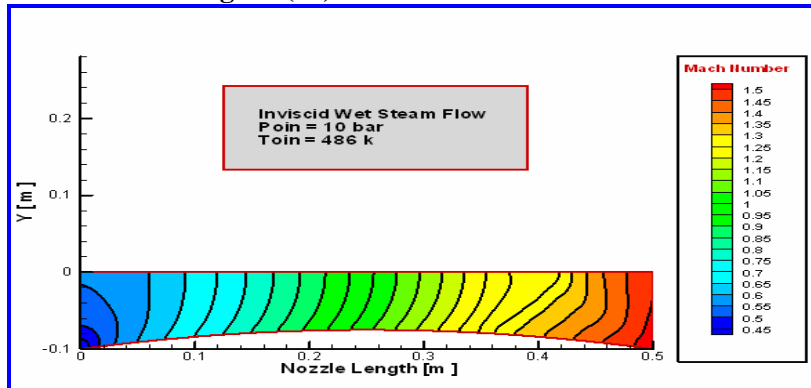
Figure (35) Mach number contours

Eng. & Tech. Journal, Vol. 27, No.13,2009

**Simulation of Spontaneous Condensation
of Viscous Steam Flow in Low-Pressure
Convergent- Divergent Nozzles**
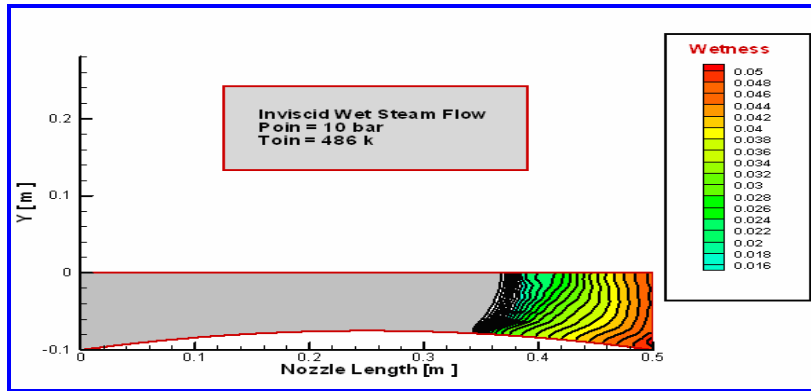
Figure (36) Wetness fraction contours
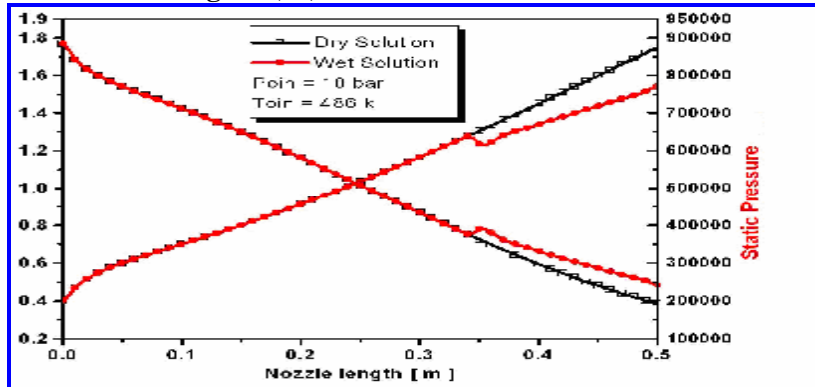
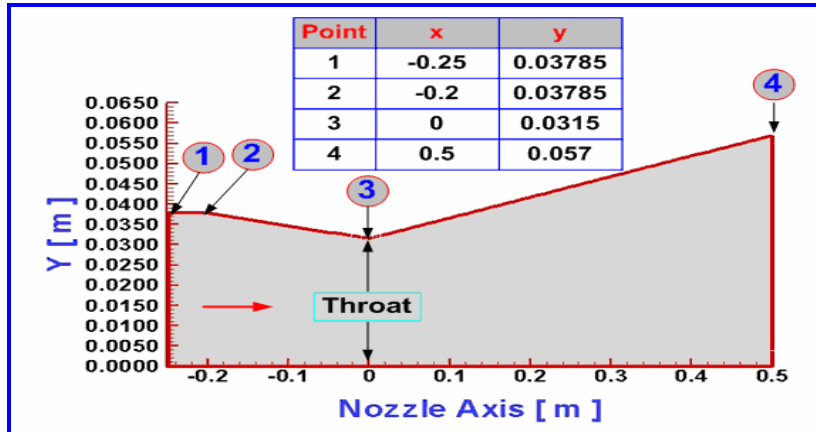**Figure (37) Comparison of pressure distribution and Mach number distribution**

Point	x	y
1	-0.25	0.03785
2	-0.2	0.03785
3	0	0.0315
4	0.5	0.057

Figure (38) Geometry of Moore nozzle

Eng. & Tech. Journal, Vol. 27, No.13,2009

Simulation of Spontaneous Condensation
of Viscous Steam Flow in Low-Pressure
Convergent- Divergent Nozzles
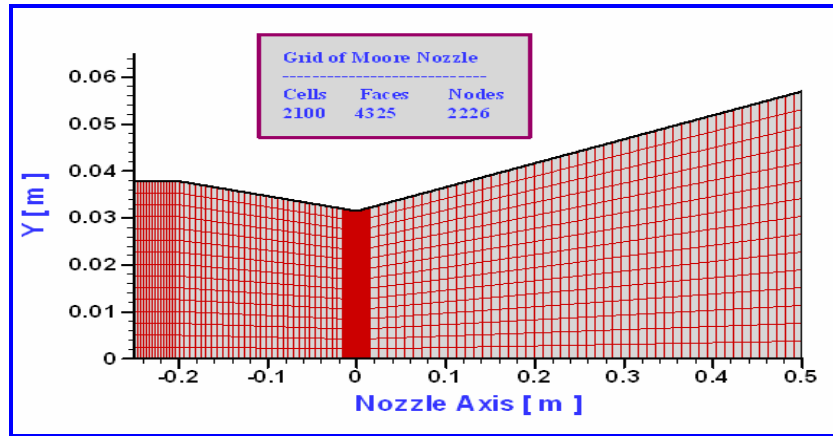
Figure (39) Grid of Moore nozzle
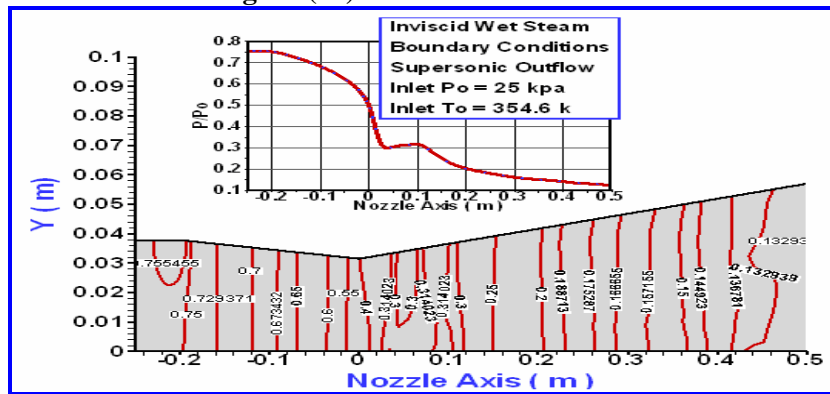
Figure (40) Isolines distribution and x-y plot of inviscid wet steam pressure ratio
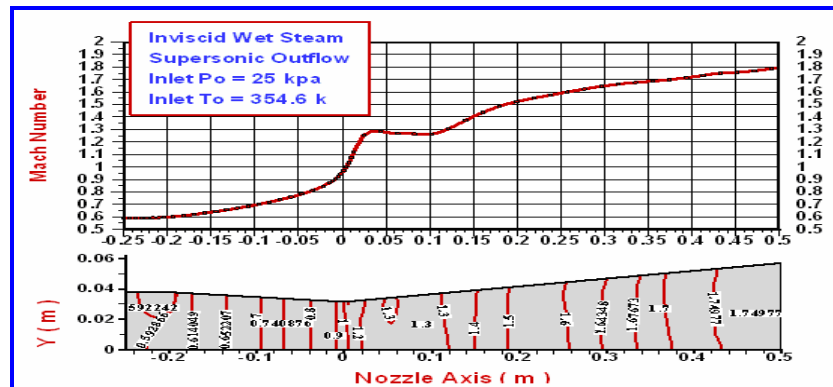
Figure (41) Mach number and isolines distribution in x-y of inviscid wet
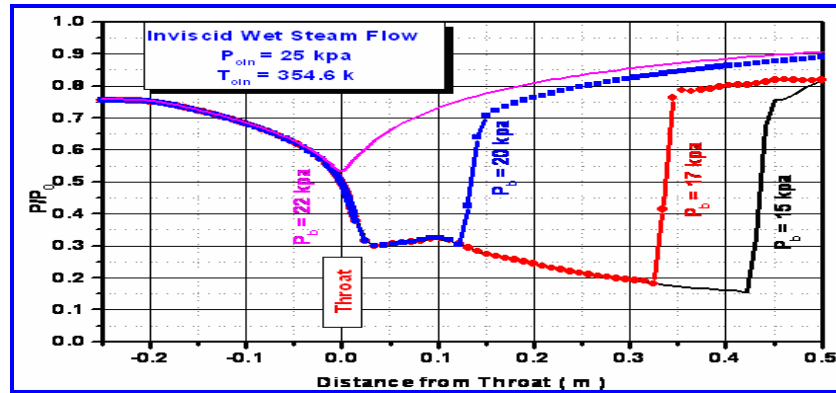
Eng. & Tech. Journal, Vol. 27, No.13,2009

Simulation of Spontaneous Condensation
of Viscous Steam Flow in Low-Pressure
Convergent- Divergent Nozzles

Figure (42) P/P_o distribution of inviscid wet steam for different back pressure values
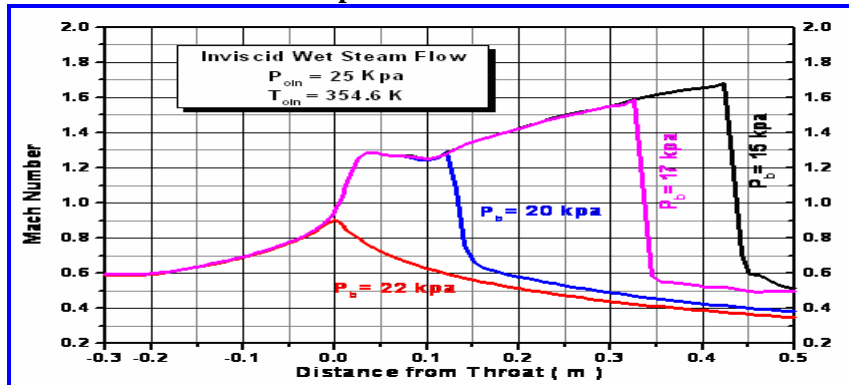
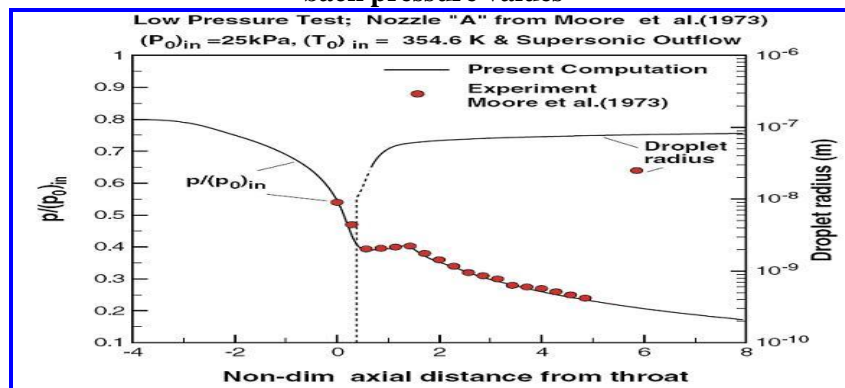**Figure (43) Mach number distribution of inviscid wet steam for different back pressure values**

Figure (44) Pressure ratio and droplet radius distributions

Eng. & Tech. Journal, Vol. 27, No.13,2009

Simulation of Spontaneous Condensation
of Viscous Steam Flow in Low-Pressure
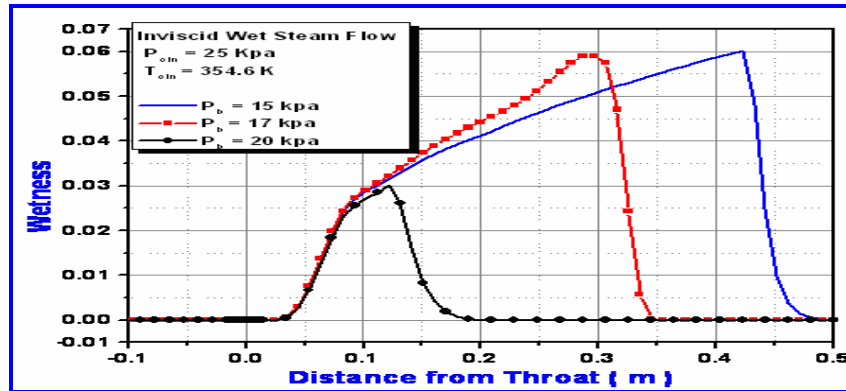Convergent- Divergent Nozzles

**Figure (45) Wetness distribution of inviscid wet steam for different back
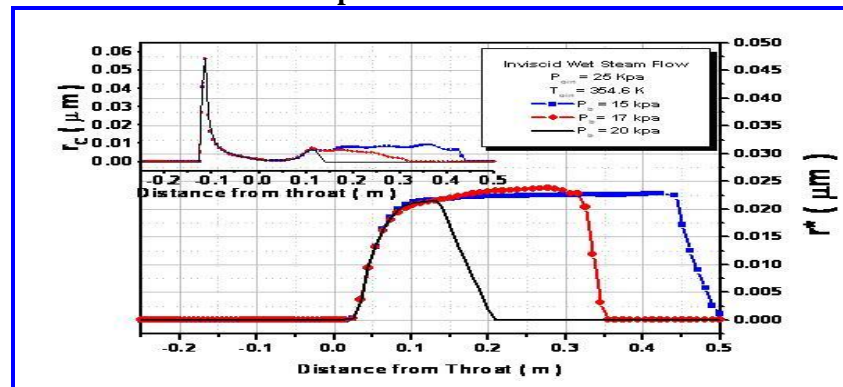pressure values**

**Figure (46) Droplet mean and critical radius distribution of inviscid wet
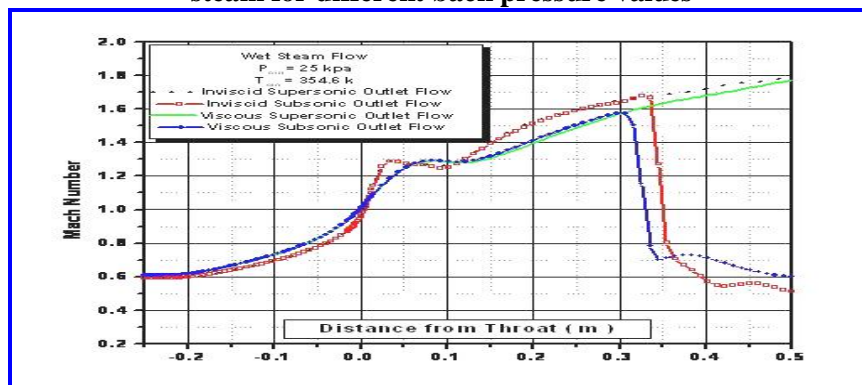steam for different back pressure values**

**Figure (47) Comparison of Mach number for inviscid wet steam at two
different outflow boundary condition situations**

Eng. & Tech. Journal, Vol. 27, No.13,2009

**Simulation of Spontaneous Condensation
of Viscous Steam Flow in Low-Pressure
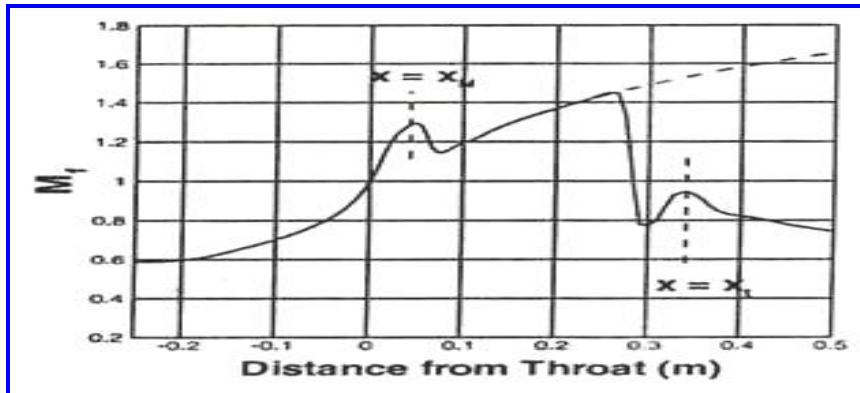Convergent- Divergent Nozzles**

**Figure (48) Comparison of Mach number for inviscid wet steam at two
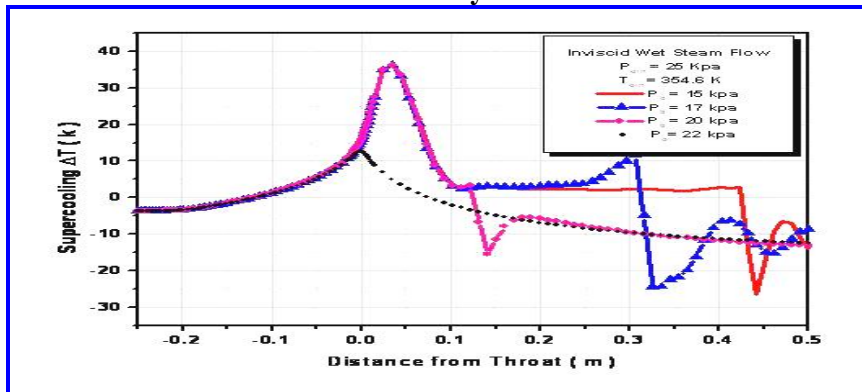different outflow boundary condition situations**

**Figure (49) Supercooling distribution of inviscid wet steam for different
outflow boundary condition situations**